A New Approach to Model Confined Suspensions Flows in Complex Networks: Application to Blood Flow

Romain Guibert, Caroline Fonta, Franck Plouraboué

DOI 10.1007/s11242-009-9492-0

A New Approach to Model Confined Suspensions Flows in Complex Networks: Application to Blood Flow

R. Guibert · C. Fonta · F. Plouraboué

Abstract The modeling of blood flows confined in micro-channels or micro-capillary beds depends on the interactions between the cell-phase, plasma and the complex geometry of the network. In the case of capillaries or channels having a high aspect ratio (their longitudinal size is much larger than their transverse one), this modeling is much simplified from the use of a continuous description of fluid viscosity as previously proposed in the literature. Phase separation or plasma skimming effect is a supplementary mechanism responsible for the relative distribution of the red blood cell's volume density in each branch of a given bifurcation. Different models have already been proposed to connect this effect to the various hydrodynamics and geometrical parameters at each bifurcation. We discuss the advantages and drawbacks of these models and compare them to an alternative approach for modeling phase distribution in complex channels networks. The main novelty of this new formulation is to show that albeit all the previous approaches seek for a *local* origin of the phase segregation phenomenon, it can arise from a *global* non-local and nonlinear structuration of the flow inside the network. This new approach describes how elementary conservation laws are sufficient principles (rather than the complex parametric models previously proposed) to provide *non local* phase separation. Spatial variations of the hematocrit field thus result from the topological complexity of the network as well as nonlinearities arising from solving a new *free boundary problem* associated with the flux and mass conservation. This network model approach could apply to model blood flow distribution either on artificial micro-models, micro-fluidic networks, or realistic reconstruction of biological micro-vascular networks.

R. Guibert · F. Plouraboué (✉)
Université de Toulouse, INPT, UPS, IMFT (Institut de Mécanique des Fluides de Toulouse),
Allée Camille Soula, 31400 Toulouse, France
e-mail: Franck.Plouraboue@imft.fr; plourab@imft.fr

R. Guibert · F. Plouraboué
CNRS, IMFT, 31400 Toulouse, France

R. Guibert · C. Fonta
Université de Toulouse, UPS, Centre de Recherche Cerveau et Cognition, Toulouse, France

R. Guibert · C. Fonta
CNRS, CerCo, Toulouse, France

Keywords Confined suspensions · Blood rheology · Apparent viscosity · Fåhræus–Lindquist effect · Phase separation · Network models

List of Symbols

μ_0	Plasma dynamic viscosity
u	Velocity field
p	Lubrication pressure field
ρ_0	Plasma density
ν_0	Plasma kinematic viscosity
Δ_c	Radial contribution of the Laplacian in cylindrical coordinates
W	Womersley dimensionless number
T	Time-scale
R	Tube radius
θ	Local relative volume of red blood cell
Q	Longitudinal flow rate
H	Discharge hematocrit
D	Tube diameter
μ_a	Apparent viscosity of blood
μ	Relative apparent viscosity of blood
H_t	Tube hematocrit
L	Tube length
J	Junction of three links i
i	Link index
C	Hydraulic conductance
μ_c	Core apparent viscosity for a large tube in microns (Kiani and Hudetz 1991)
δ	Width of marginal layer in microns (Kiani and Hudetz 1991)
d_m	Effective diameter of one red blood cell in a small tube (Kiani and Hudetz 1991)
$\mu_{0.45}$	Relative apparent viscosity for $H = 0.45$ (Pries et al. 1990)
c	Parameter of Pries et al.'s (1990) model
n_i	Number of input nodes
n_o	Number of output nodes
n_{int}^{I}	Number of internal inflow nodes
n_{int}^{O}	Number of internal outflow nodes
n_{int}^{U}	Number of internal undetermined nodes
f	Subscript for the incoming branch of an inflow junction
α	Subscript for an outgoing branch of an inflow junction
β	Subscript for an outgoing branch of an inflow junction
κ	Generic subscript for α or β
γ_κ	Fractional blood flow entering κ-branch at the inflow junction
θ_κ	Fractional discharge hematocrit entering κ-branch at the inflow junction
m	Empiric parameter for Dellimore et al.'s (1983) phase separation model
a	Plasma skimming parameter (Fenton et al. 1985a,b)
d_c	Size of red blood cell Fenton et al.'s model (1985a; 1985b)
I	Internal inflow node
O	Internal outflow node
U	Internal undetermined node
H_N	Node hematocrit

L_i Set of internal nodes linked to input nodes n_i
h_0 Input hematocrit

1 Introduction

Two-phase flows in porous media generally refer to the flow of two immiscible fluids inside a porous solid matrix (Barenblatt et al. 1990). There is nevertheless another class of problems which is more rarely considered within the same vocabulary : the flow of a suspension of dispersed solid/particle phase flowing within a liquid inside a porous medium. Albeit different from polymer flows in porous media, such two-phase flows share some important common properties. Both of them display nonlinear relationship between the concentration of the disperse phase (polymer or particles) and the rheological parameters of the flow (Entov and Rozhkov 1985). These non linearities are very sensitive to the structuration of the dispersed phase at the "microscopic" level. Moreover, if at the "microscopic" level the polymer chain's length or the particle size is comparable with the pore size, it is then questionable to seek for a continuum mechanics description of such a dispersed flow.

This question has been challenging since a long time when considering the modeling of blood flow in small capillary vessels. From the fluid mechanical point of view, blood is merely a suspension of red blood cells since they represent 99% of blood cell content. The non-cellular part of the blood is the plasma whose rheological properties are close to water. Red blood cells are biconcave disks the diameter of which is 7–8 microns in their larger dimensions and 2 microns in their thinner ones. Since the thinnest capillaries diameters in most mammalian bodies are close to 5 microns, one can see that particle size and pore size are of the same order for this class of flows. Hence, there is an intrinsic difficulty in the application of macroscopic continuum non-Newtonian rheological models of the blood to describe its flow within micro-circulation. This long-standing question has motivated intense research efforts over the last four decades to settle reliable models for confined blood flow (Fung 1973; Popel and Johnson 2005; Lee and Smith 2008).

Moreover, the dispersed flow of plasma and red blood cells within a long tube-like vessel is only confined within the transverse direction. Hence, it is generally worth considering that the tube length is larger than the particle size along the longitudinal direction. The same considerations also apply in micro-fluidic network channels, for which the channel length is generally much longer than their width. In this case, a continuum mechanic approach can still hold to describe the longitudinal pressure variations. Furthermore, even if the solid phase (polymer or particles) can be confined in the transverse direction, the fluid phase into which it is dispersed can always be considered as continuous. Indeed, many experimental researches have analyzed the blood flux induced by a given pressure drop inside a small capillary tube. As a result of using the analogous Poiseuille law, these measurements have permitted the evaluation of the blood apparent viscosity which is generally defined relatively to the plasma viscosity (Chien et al. 1985; Cokelet 1999). The early experiments of Fåhræus and Lindquist (1931) have already led to the conclusion that this apparent viscosity decreases as the tube diameter decreases (as observed on the right part of Fig. 1a—a fairly unexpected result at the time). The mechanism responsible for the so-called Fåhræus–Lindquist effect, i.e., the reduction of the apparent viscosity when increasing the blood transverse confinement is the lubrication of red blood cells by plasma. The structuration of the flow associated with hydrodynamic forces centers the red blood cells so that the viscous dissipation effects are minimized when the plasma acts as a lubricant to the red

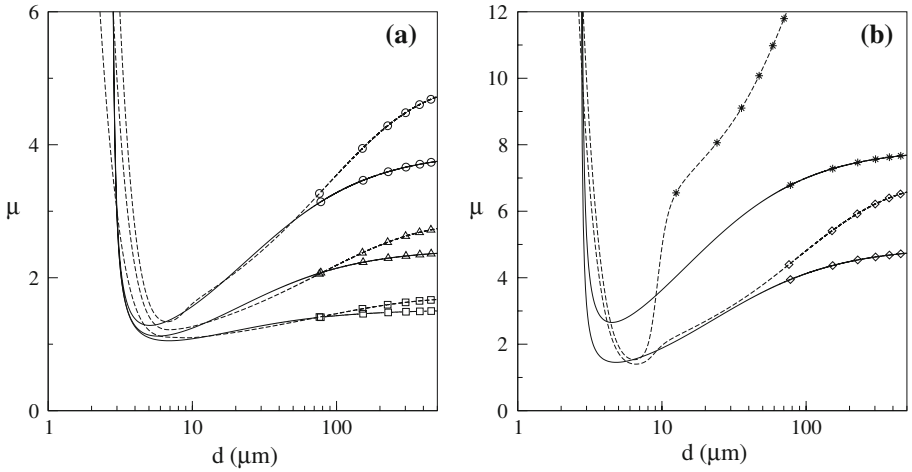

Fig. 1 Blood relative apparent viscosity function of tube diameter using Kiani and Hudetz (1991) (*continuous lines*) and Pries et al. (1990) (*dashed lines*) viscosity laws for different inlet hematocrits: **a** $H = 0.2$ (*square*), $H = 0.4$ (*triangle*) and $H = 0.6$ (*circle*), **b** $H = 0.7$ (*diamond*) and $H = 0.9$ (*star*)

blood cells' flow. However, when the tube diameter reaches a size close to the smallest dimension of red blood cells, a marked increase of the apparent viscosity is observed. This dramatic increase of the apparent viscosity is associated with the viscous dissipation in the thin lubrication films which are formed between the deformed particles and the wall (Lighthill 1968).

It has been more recently realized that it was also associated in vivo with the compression of the glycocalyx which lies at the surface of endothelial cells (Damiano et al. 1996; Feng and Weinbaum 2000). Even though the mechanisms are known, the elaboration of a complete model for the apparent viscosity of blood over the whole range of diameters and hematocrits (the red blood cells' relative volume inside vessels) parameters heavily relies on phenomenological models which describe experimental data (Pries et al. 1986, 1989; Kiani and Hudetz 1991; Kiani et al. 1994; Popel et al. 1988). We will detail these models in Sect. 2.

Another important effect associated with the hydrodynamic interactions between the dispersed red blood cells' phase, the plasma and the capillaries is the so-called plasma skimming effect or phase separation. When studying the in vivo distribution of the hematocrit into the daughter branch of a given bifurcation, it has been observed that its relative distribution was generally non-symmetrical (even if the diameters of the daughter branches were merely identical), suggesting some complex hydrodynamical coupling to hold at the local scale. This effect is generally described as the structuration of the flow arising at each bifurcation of the capillary network. It leads to an asymmetric distribution of red blood cell concentration along each daughter branch of a given bifurcation. This phenomenon has received considerable attention since it is an important ingredient for the modeling of the red blood cells (and thus oxygen) distribution inside capillary networks (Dellimore et al. 1983; Fenton et al. 1985a,b; Pries et al. 1990).

Physiologists have then proposed a number of phenomenological models to describe this "phase separation" to provide a reliable and quantitative prediction to it.

A complete, detailed physical understanding of the mechanism at hand in those models is still missing in the existing literature. Nevertheless, some recent in vitro experiments (Faivre et al. 2006) and their theoretical analyses have provided evidences showing that plasma

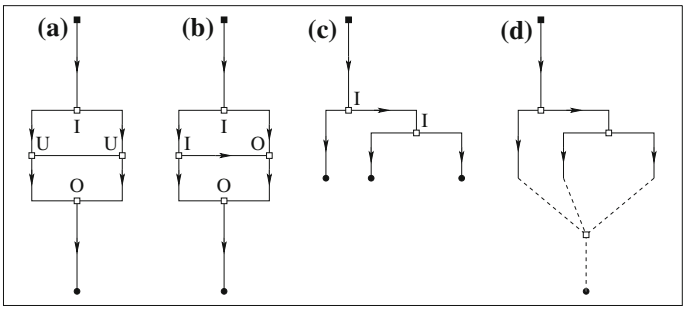

Fig. 2 Definition of the different categories of nodes which have to be considered. *Black squares* represent input nodes n_i whilst *black circles* represent output nodes n_o. *White squares* represent internal nodes n_int, the quality of which is indicated with a *capital letter*. I stands for "inflow" node (1 influx branch, 2 outflux ones), O for outflow node (2 influx branches, 1 outflux one) and U for undetermined. The *arrows* indicate the direction of the flow in each link or branch. **a** $n_\mathrm{i} = n_\mathrm{o} = 1$, $n_\mathrm{int} = 4$, $n^\mathrm{I}_\mathrm{int} = n^\mathrm{O}_\mathrm{int} = 1$, $n^U_\mathrm{int} = 2$; **b** $n_\mathrm{i} = n_\mathrm{o} = 1$, $n_\mathrm{int} = 4$, $n^\mathrm{I}_\mathrm{int} = n^\mathrm{O}_\mathrm{int} = 2$, $n^U_\mathrm{int} = 0$; **c** $n_\mathrm{i} = 1$, $n_\mathrm{o} = 3$, $n_\mathrm{int} = n^\mathrm{I}_\mathrm{int} = 2$, $n^\mathrm{O}_\mathrm{int} = n^U_\mathrm{int} = 0$; **d** $n_\mathrm{i} = 1$, $n_\mathrm{o} = 1$, $n_\mathrm{int} = n^\mathrm{I}_\mathrm{int} = 2$, $n^\mathrm{O}_\mathrm{int} = n^U_\mathrm{int} = 0$. The *dotted lines* indicate some virtual link which have to be considered for imposing the output boundary condition (42) when transforming the output nodes number $n_\mathrm{o} > 1$ of (**c**)

skimming arises from the hydrodynamic drift of non-spherical cells in shear flow. Moreover, recent numerical simulations also demonstrate that hydrodynamical interactions are responsible for the cell structuration inside microcapillaries (McWhirter et al. 2009).

Before giving the details of the proposed models in Sect. 2.2, it is important to mention that they all apply to "inflow" bifurcations but not to "outflow" ones (as described in Fig. 2). Such discrimination between "inflow" and "outflow" bifurcations justifies the vocable "separation" effect since it does suggest that a mother hematocrit has to be distributed into daughter branches, so that it separates the red blood cell inflow into both of them.

Different models have been proposed in the literature the detail of which is reviewed in Sect. 2. A common point of view shared by these models is that the phase separation mechanism comes from the complex interplay of geometrical and hemodynamics interaction *at the local level* of each bifurcation. It is very important to stress that the in vivo experimental data associated with the elaboration of these models have been obtained from selecting single bifurcations among a complex network (Pries et al. 1989, 1990, 1992). Some efforts have been made to better quantify the origin of the phase separation phenomenon either from the analysis of numerical simulations (Enden and Popel 1994) or detailed fluid-mechanical interactions (El-Kareh and Secomb 2000) arising at the level of a single bifurcation. More recent investigations have addressed the influence of separation effect on the dynamical behavior of very simple networks (Carr and Lacoin 2000; Carr et al. 2005; Pop et al. 2007). Nevertheless, all the above mentioned contributions always consider that phase separation results from *local* mechanisms, and as such, should be modeled by *local* laws.

In this article, we show that local mechanisms are not a necessary condition to obtain phase segregation in complex networks. We adopt the complementary point of view that such phase segregation results from non-local interactions associated with the topological complexity of networks and conservation laws when using proper boundary conditions. This new formulation is proposed in Sect. 3 where a detailed description of its numerical implementation is given. Finally, we compare our new approach with local models in Sect. 4. This section shows that the previously proposed phenomenological models display a number of drawbacks that our formulation avoid when considering a network with heterogeneous conductances.

2 Constitutive Equations for Confined Blood Flow

Let us assume that the flow of suspension is steady and governed by the Poiseuille law. Then, the presence of the particles in suspension leads to an apparent viscosity μ_a which differs from the plasma one μ_0 and depends on the dynamic red cell fraction H (which is called the hematocrit) as well as the channel diameter. For the steady-state flow, the total flow rate is constant. The concentration of particles H_t and the dynamic concentration H are also constant in time and space as one has no positive or negative sources of red cells. The detailed derivation of these considerations is presented in Sect. 2.1 which might be skipped in a first reading of this article. One then needs to know :

- The dependence of the apparent viscosity upon the hematocrit and the tube diameter which is given in the first paragraph section 2.2.
- The hematocrit distribution along each bifurcation which is given in the second paragraph of Sect. 2.2.

2.1 Lubrication Approximation

This section elaborates the constitutive relations associated with confined particles dispersed within a fluid of dynamic viscosity μ_0.

These constitutive equations are based upon the hypothesis that the flow occurs within high-aspect ratio tube-like channels. Furthermore, it will be assumed (following Pop et al. 2007) that the particle suspension can be described by a continuous void fraction θ, so that the fluid has continuous properties everywhere. Let us consider the longitudinal velocity component $u(r, z, t)$ and the associated lubricated pressure $p(z, t)$, at radial and longitudinal positions r and z, in the cylindrical coordinate systems (r, ϕ, z).

It is worth noting that, as usual (Leal 1992), the lubricated pressure $p(z, t)$ does not depend on the radial coordinate r. We first consider within this analysis each vascular segment as a single unit into which the lubrication equations are written in the plasma region:

$$\frac{\partial u}{\partial t} = -\frac{1}{\rho_0}\frac{\partial p}{\partial z} + \nu_0\, \Delta_c u, \tag{1}$$

where ρ_0 is the fluid density, ν_0 the plasma kinematic viscosity, and $\Delta_c \equiv (1/r)\, \partial_r(r \partial_r)$ stands for the radial contribution of the Laplacian in cylindrical coordinates and the incompressibility condition

$$\operatorname{div} \mathbf{u} = 0. \tag{2}$$

The dimensionless form of Eq. 1 can be written as

$$W^2 \frac{\partial u^*}{\partial t^*} = -\frac{\partial p^*}{\partial z^*} + \Delta_c^* u^*. \tag{3}$$

This dimensionless equation, where the symbol $*$ is associated with dimensionless variables, provides the Womersley number $W = R/\sqrt{T\nu_0}$ based on a typical time-scale T, the uniform tube radius R, and the plasma kinematic viscosity. From the realization that the shortest time-scale associated with the heart pressure pulses is $T = 0.1\,\mathrm{s}$ (Kleinfeld et al. 1998), or with the vascular tube regulation is $T = 1\,\mathrm{s}$ (Devor et al. 2008), one then realizes that vessels having a 10 micron radius $R = 10^{-5}\,\mathrm{m}$ experiences very weak viscous dynamical effects since $W \simeq 10^{-2}$.

Hence, at the capillary scale, the Womersley number is so small that the fluid flow instantaneously responds to the hydrodynamical variations. These variations are in particular related

to the presence of the solid phase within the tube which locally squeezes-out the plasma along the tube walls. This dimensionless formulation of the momentum balance was useful to show that the stationary limit of the lubrication equations is a reasonable approach for micro-channel flows. In the following. we keep with a dimensional formulation of the problem to provide dimensional quantities that could be more easily related to real experimental network configurations.

According to Pop et al. (2007) and their associated notations, we consider the local relative volume of red blood cell $\theta(r, z, t)$ at location r and z, for which the dynamical behavior is related to the mass conservation laws given by the equation:

$$\frac{\partial \theta}{\partial t} + u \frac{\partial \theta}{\partial z} = 0. \tag{4}$$

Relations (3) and (4) are the dynamical equations governing the local fluid velocity, the local hematocrit, and the pressure. From now, taking into consideration the $W \to 0$ limit of relation (3) integrated along the radial direction, it is possible to deduce a simple relation between the longitudinal flux:

$$Q = 2\pi \int_0^R u(r)\, r \, \mathrm{d}r, \tag{5}$$

and the discharge hematocrit H defined by

$$H(z, t) = \frac{2\pi}{Q} \int_0^R \theta(r, z, t)\, u(r)\, r \, \mathrm{d}r, \tag{6}$$

associated with the stationary pressure/flux relationship

$$Q = -\frac{\pi}{128} \frac{D^4}{\mu_{\mathrm{a}}(H, D)} \frac{\partial p}{\partial z}, \tag{7}$$

where

$$\mu_{\mathrm{a}}(H, D) = \mu_0\, \mu(H, D). \tag{8}$$

The averaged relation (7) describes a modified linear relationship between the pressure drop and the flux which obviously results from the local linear lubrication flows. It introduces an effective viscosity coefficient which takes into account the presence of the particles in the flow. However, the detailed derivation of this relation needs the evaluation of cumulative pressure drop in the plasma films squeezed by the presence of the particles. It cannot simply be obtained by an average of (1), but needs the resolution of the pressure field in different regions to match one with another to get the total pressure drag which can be evaluated for simple particle shapes (Lighthill 1968). It is important to mention that this relation heavily relies on the lubrication hypothesis. It ignores the complex three-dimensional Stokes effect which locally arises in the vicinity of each bifurcation over a length-scale which is of the order of a few tube diameters. Furthermore, extensive experimental phenomenological laws have also been proposed to describe the dependence of the relative apparent viscosity $\mu(H, D)$ on the discharge hematocrit H and the tube diameter $D = 2R$ that will be detailed in the next section.

The discharge hematocrit H which results from a velocity-weighted averaged mass flux is the red blood cells' volume fraction which would result from extracting the blood flow in a

cup and measuring its cell volume fraction (the equivalent of the "mixing cup" average found in convective thermal problems, and also from the fractional flow in the Buckley–Leverett theory of two-phases immiscible flow through porous media).

The fluid incompressibility then leads to

$$\frac{\partial Q}{\partial z} = 0. \tag{9}$$

Again, based on Pop et al. (2007) and from surface-averaging relation (4), it is possible to get the flux–hematocrit relationship using (9)

$$\frac{\partial H_\mathrm{t}}{\partial t} + \frac{\partial H}{\partial z} Q = \frac{\mathrm{d}H_\mathrm{t}}{\partial t} + \frac{\partial (HQ)}{\partial z} = 0, \tag{10}$$

where $H_\mathrm{t}(z,t)$ is the surface average of θ also called the tube hematocrit

$$H_\mathrm{t}(z,t) = \frac{2}{R^2} \int_0^R \theta(r,z,t)\, r\, \mathrm{d}r. \tag{11}$$

That this tube hematocrit differs from the flux–hematocrit is a long-standing observation called the Fåhræus effect in the literature (Popel and Johnson 2005). The relationship between $H_\mathrm{t}(z,t)$ and H depends on the micro-scale particles/flow configuration θ. There is a general agreement in the literature for a nonlinear relationship $H_\mathrm{t}(z,t) = H_\mathrm{t}(H(z,t))$, and some models have been proposed (Pries et al. 1996; Pop et al. 2007). From Fåhræus effect and incompressibility (9), it is interesting to write (10) as

$$\frac{\partial H}{\partial t} + Q \frac{\mathrm{d}H}{\mathrm{d}H_\mathrm{t}} \frac{\partial H}{\partial z} = 0, \tag{12}$$

to realize that it describes a one-dimensional convective transport of the discharge hematocrit H along the tube axis, at velocity $Q \frac{\mathrm{d}H}{\mathrm{d}H_\mathrm{t}}$. One can then realize that the red blood cells are not transported at the plasma mean flux Q, but at a relative flux $\frac{\mathrm{d}H}{\mathrm{d}H_\mathrm{t}} Q$. This observation could contradict relation (4) which describes a local convection of the local hematocrit at the plasma velocity. This is because the particles are not homogeneously placed inside the flow, but preferentially in the center of the tube where they experience higher flows, so that their average flow transport differs from those of the fluid.

If we now consider the stationary limit of the integrated constitutive equation (10), one then realizes that the hematocrit has to be constant along each vascular segment, so that H is not a function of z and t anymore, in the same way as the flux Q. This property of the stationary solution does not depend on the Fåhræus effect.

When integrating relation (7) in this stationary limit along each vessel segment, one can then deduce the relationship between the pressure drop between two successive bifurcations Δp, the apparent viscosity μ_a, the segment length L, and the flux Q

$$Q = -\frac{\pi}{128} \frac{D^4}{\mu_\mathrm{a}(H,D)} \frac{\Delta p}{L}. \tag{13}$$

This relationship is the cornerstone of a discrete network method to compute the pressure distribution inside very complex networks since the continuous mechanical equations have been integrated analytically within an asymptotic formulation to obtain this discrete version as in Plouraboué et al. (2006). It is important to realize that this relationship also ignores Stokes pressure drop contributions coming from the complex flow in the vicinity of each bifurcation. Since these Stokes corrections to the lubrication approximation are localized

within a distance R from the bifurcation, the contribution of these effects on the pressure drop Δp is of order $O(R/L)$. Since the ratio R/L in almost all vascular networks is of the order of $1/20$ (Risser et al. 2009), the expected correction associated with the three-dimensional complex flow at bifurcation is expected to be as small as 10% and should then safely be discarded.

From the conservation law written in another form (9) and (13) for the sets of vascular segments i associated with a given junction J, we arrive at the following discrete sets of equations for the pressure and hematocrit of a complex network

$$\sum_{i\in J} Q_i = -\sum_{i\in J} C_i(D_i, H_i)\,\Delta_i p = -\sum_{i\in J} \frac{\pi}{128}\frac{D_i^4}{\mu_{\rm a}(H_i, D_i)}\frac{\Delta_i p}{L_i} = 0, \tag{14}$$

where the flux Q_i in each branch (each link related to the junction J) is taken to be positive for influx and negative for out-flux (this is the Kirchhoff's law for electrical circuits). $\Delta_i p$ stands for the pressure difference between the central node minus each adjacent ones, and C_i is the hydraulic conductance of each branch. From the integration of the stationary limit of relation (10) we also arrive at

$$\sum_{i\in J} H_i\, Q_i = 0. \tag{15}$$

This mass conservation for the hematocrit is again established when neglecting complex three-dimensional hydrodynamic effects arising in the vicinity of each bifurcation.

As for the previous incompressibility condition, (14), such correction should be of order $O(R/L)$ so that it will lead to a negligible correction for micro-vascular networks.

It is worth noting that, from now on, no additional hypothesis rather than momentum balance, mass conservation, fluid incompressibility, and lubrication approximation would be used to establish the discrete network formulation equations (14) and (15). Furthermore, it is also interesting to note at this stage, that, if some homogeneous input hematocrit h_0 is injected in the network, then the homogeneous trivial solution, $H_i = h_0$, is always a possible solution. This comes from the fact that factorizing an homogeneous hematocrit value in (15) leads to flux conservation which is automatically verified from (14). This is nevertheless not an interesting one since it is generally not the one which is observed in experiments. This is why we consider other possible solutions, either from using additional local "segregation models," or by developing a new formulation.

2.2 Phenomenological Models for Blood Flow

2.2.1 Apparent Viscosity

The first important supplementary ingredient which is needed to describe the flow of confined suspensions in channels is the knowledge of the apparent viscosity. Previous theoretical attempts toward this direction are longstanding since Lighthill's (1968) study where it is realized that the viscous drag on elastically deformable spherical objects is mainly concentrated in thin regions, the precise contribution of which could be computed from matching techniques. Nevertheless, the resulting drag coefficient depends on the detail of the deformation of the particle suspension. For non-deformable spherical object, it can be safely computed, but for object as complicated as red blood cells, it is much more difficult to evaluate. Since then, many other efforts have been dedicated to the accurate computation of the coupled Stokes flow around axisymmetrical red blood cells using complex membrane rheological models (see Quéguiner and Barthès-Biesel 1997, for example).

More recently, it has been pointed out that when the red blood cell is very much confined in vivo into small capillary vessels, it can experience a supplementary drag coming from the compression of the glycocalyx layer (Damiano et al. 1996; Feng and Weinbaum 2000). Hence, depending on the specific particles and the precise channel into which they are confined, the precise apparent viscosity law can change. From now on, we will restrict our interest to models that have been proposed to describe the experimental results associated with blood flow into in vitro cylindrical tubes. Nevertheless, the approach which is proposed in Sect. 3 is rather generic and can also be adapted to other contexts using the proper apparent viscosity law.

Kiani and Hudetz (1991) have proposed a semi-empirical model based on hydrodynamical considerations associated with the lubrication of red blood cells by plasma. The apparent viscosity of this model which depends on the discharge hematocrit H and on the tube diameter D is given by

$$\mu(H, D) = \left(1 - \left(1 - \frac{\mu_0}{\mu_c}\right)\left(1 - \frac{2\,\delta}{D}\right)^4\right)^{-1}\left(1 - \left(\frac{d_m}{D}\right)^4\right)^{-1}, \tag{16}$$

where μ_c represents the blood viscosity in large vessels and is given by the following empirical law:

$$\mu_c = \exp^{(0.48+2.35\,H)}. \tag{17}$$

Parameter δ represents the thickness of the marginal plasma layer which lubricates red blood cells and is given in microns by

$$\delta = 2.03 - 2\,H. \tag{18}$$

Finally, parameter d_m represents the maximal size of deformation of a red blood cell and is deduced from experimental observation to be equal in micron units to

$$d_m = 2.7. \tag{19}$$

The advantage of the Kiani–Hudetz model over others is that it could be parameterized for suspensions other than blood because each given parameter has a physical interpretation.

Another popular model for confined blood rheology is the one proposed by Pries et al. (1990, 1996) to describe the in vitro relative apparent viscosity. On the contrary to the previous one, this model is based on a number of phenomenological parameters the interpretation of which is not easy (see Pries et al. (1996) for more details on the interpretation of parameters $\mu_{0.45}$ and c). The relative apparent viscosity is given by

$$\mu(H, D) = 1 + (\mu_{0.45} - 1)\,\frac{(1-H)^c - 1}{(1-0.45)^c - 1}, \tag{20}$$

$$\mu_{0.45} = 200\,\exp^{(-1.3\,D)} + 3.2 - 2.44\,\exp^{(-0.06\,D^{0.645})}, \tag{21}$$

$$c = \left(0.8 + \exp^{(-0.075\,D)}\right)\left(-1 + \frac{1}{1 + 10^{-11}\,D^{12}}\right) + \frac{1}{1 + 10^{-11}\,D^{12}}. \tag{22}$$

Surprisingly enough, when considering the difference between both formulations, they provide consistent viscosities in the range of the most meaningfully physiological parameters as illustrated in Fig. 1a. However, when the hematocrit reaches values as high as 0.7, both models display distinct differences in the apparent viscosity, especially for large vessel diameters as shown in Fig. 1b. For hematocrit values as large as 0.9, the validity of the values given by the models is questionable, as also illustrated on Fig. 1b.

2.2.2 *Plasma Skimming Laws or Phase Separation Effect*

All the above considerations are restricted to networks having only three-branched junctions called bifurcations, and "inflow" configurations. We will see below that some supplementary relationships are needed to describe the "outflow" bifurcations to close the set of equations associated with the determination of pressure and hematocrit in a complex network. It is also important to mention that all the above sets of equations have been elaborated in the context of stationary flows, so that a direct application to dynamical formulations as done in Carr and Lacoin (2000); Carr et al. (2005) and Pop et al. (2007) should be taken with caution.

From now on, we denote the mother incoming branch with a m subscript and the daughter outgoing branches with subscripts, α and β.

Based on the clear notations of Pop et al. (2007), the models can be synthetically described using the fractional outgoing flow

$$\gamma_\kappa = Q_\kappa / Q_\mathrm{m}. \tag{23}$$

The subscript κ is equal to either α or β. Mass conservation (14) implies

$$Q_\alpha + Q_\beta = Q_\mathrm{m}, \tag{24}$$

so that one of the fractional flux is a trivial function of the other one

$$\gamma_\beta = 1 - \gamma_\alpha. \tag{25}$$

The other quantity to consider is the fractional discharge hematocrit

$$\theta_\kappa = H_\kappa / H_\mathrm{m} \tag{26}$$

Plasma skimming models then provide the dependence of the fractional discharge hematocrit θ_κ with the fractional flux and, for some of them, other parameters such as the diameters of the branches. We hereby detail three different skimming models proposed by Dellimore et al. (1983), Fenton et al. (1985a; 1985b), and Pries et al. (1989; 1990).
The hypotheses of those models differs depending on which parameters are considered to influence the fractional discharge hematocrit θ_κ.

Dellimore et al. (1983) propose that the fractional hematocrit fulfils the following power law versus the fractional flux:

$$\theta_\kappa(\gamma_\kappa) = \frac{{\gamma_\kappa}^{m-1}}{{\gamma_\kappa}^{m} + (1-\gamma_\kappa)^m}, \tag{27}$$

where the phenomenological parameter m is chosen to be equal to $m = 1.2$. From this relation, it is easy to verify that the mass conservation (15) when using (25) can be expressed as

$$\theta_\alpha \gamma_\alpha + \theta_\beta (1-\gamma_\alpha) = 1. \tag{28}$$

Fenton et al. (1985a,b) propose the following model:

$$\theta_\kappa(\gamma_\kappa, D_\mathrm{m}) = a + \frac{1-a}{2\gamma_\kappa}, \tag{29}$$

$$a = \frac{1}{1.4 - \sqrt{d_\mathrm{c}/D_\mathrm{m}}}, \tag{30}$$

where d_c is related to the red blood cell size, and a is greater than or equal to 1. The parameter d_c is not specified in each publication, and its value ranges from 5 to 8 μm. In the subsequent

computations, we will choose the value $d_c = 5\,\mu m$. Again, this model verifies the conservation equation (28).

Pries et al. (1989, 1990) have proposed the following more elaborated model:

$$\theta_\kappa(\gamma_\kappa, D_\alpha, D_\beta, D_m) = \frac{1}{\gamma_\kappa} \begin{cases} F_\kappa(\gamma_\kappa, D_\alpha, D_\beta, D_m) & x_0 < \gamma_\kappa < 1 - x_0 \\ 0 & \gamma_\kappa \leq x_0 \\ 1 & \gamma_\kappa \geq 1 - x_0 \end{cases} \tag{31}$$

where

$$F_\kappa(\gamma_\kappa, D_\alpha, D_\beta, D_m) = \frac{1}{1 + \exp\left(A_\kappa - B \ln G_\kappa\right)}, \tag{32}$$

for which

$$G_\kappa(\gamma_\kappa) = \frac{\gamma_\kappa - x_0}{1 - \gamma_\kappa - x_0}, \tag{33}$$

and

$$B = 1 + 6.98\left(\frac{1 - H_m}{D_m}\right), \quad x_0 = \frac{0.4}{D_m}, \quad A_\alpha = -A_\beta = \frac{6.96}{D_m} \ln\left(\frac{D_\alpha}{D_\beta}\right). \tag{34}$$

It is also possible to verify that this model fulfills the mass conservation equations (28). It is important to note that all these models provide two relations for the fractional hematocrit of each daughter branch of inflow bifurcations. For "outflow" bifurcations, only a single relation associated with the mass conservation (28) is imposed. Hence, there is a distinct difference between "inflow" and "outflow" bifurcations in these models, and a supplementary information is given in the first case which relies on the hypothesis that the phase separation occurs from a local mechanism.

The fractional hematocrit of the three models is presented in Fig. 3a and b. They all present similar variations with a first increase of the hematocrit ratio versus the corresponding flux ratio. Nevertheless, some details of the curve differ when varying certain parameters such as a zero plateau for the hematocrit ratio for the smallest γ_α values or the presence of a maximum for large γ_α values. One important common feature of these models is the possibility for the daughter branch to reach an hematocrit value larger than the mother one (when the hematocrit ratio is larger than one). Such feature has been observed experimentally (see, for example, Fig. 4 of Pries et al. (1989)), and it is found in highly asymmetrical bifurcations for which the flux distribution is predominantly going into one of the daughter branch when it is, therefore, needed. From relation (28), if $\theta_\alpha < 1$, then $\theta_\beta > 1$ and vice-versa. It can also be observed on Fig. 3b that the model proposed in Fenton et al. (1985b) displays undesirable negative hematocrits at low relative flux values. This is a problem of this early model, and much later, another one such as Pries et al. (1989) cures this drawback by prescribing a zero value at low γ_α as observed in the continuous lines set of Fig. 3a.

This common property of the models can lead to undesirable effects in some networks where some of the hematocrits at a given link can reach values that are larger than one as will be seen in Sect. 4.

In the next section, we present an alternative formulation which treats equally inflow and outflow bifurcations and provides phase separation from a global coupling effect.

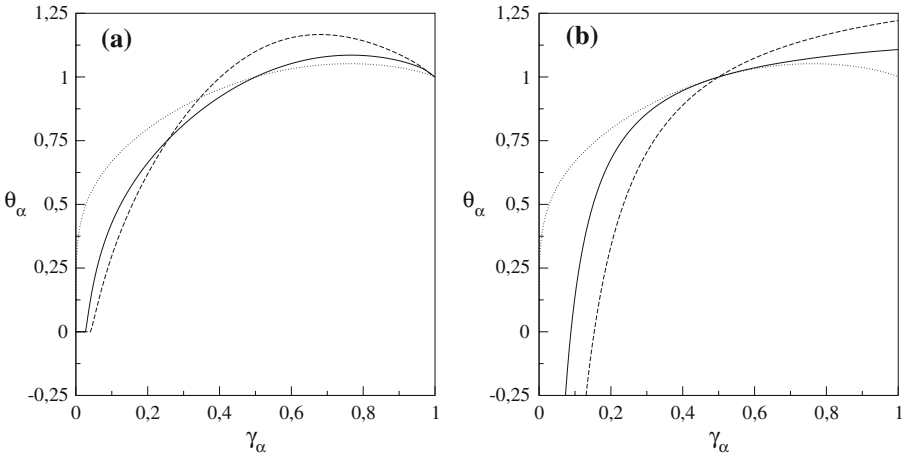

Fig. 3 Fractional discharge hematocrit θ_α versus the Fractional blood flow γ_α for the various phase separation models used. Two configurations are tested: $d_\mathrm{m} = d_\alpha = d_\beta = 15\,\mu\mathrm{m}$ (*continuous lines*) and $d_\mathrm{m} = 20\,\mu\mathrm{m}$, $d_\alpha = 10\,\mu\mathrm{m}$, $d_\beta = 15\,\mu\mathrm{m}$ (*dashed lines*). Dellimore et al.'s (1983) model (*dotted line*) is represented on the two *graphs* as reference, **a** Pries et al.'s (1990) model with *continuous lines* and **b** Fenton et al.'s (1985a; 1985b) model with *continuous lines*

3 New Formulation for the Computation of Confined Suspensions in Complex Networks

3.1 Theoretical Formulation

3.1.1 Previous Formulations

Let us now describe in more detail a theoretical description of confined suspension models associated with the previous formulations. We did not find in the literature a detailed description of the close set of equations to be solved in complex networks. This is why we describe it in this first paragraph.

Let us introduce a general complex network having n nodes associated with either bifurcations or input/output nodes. Among the total n nodes let us distinguish n_i input nodes, n_int internal nodes and n_o output nodes, as illustrated in Fig. 2, and by definition

$$n = n_\mathrm{i} + n_\mathrm{int} + n_\mathrm{o}. \tag{35}$$

Furthermore, in an oriented graph, one should also consider, among the internal nodes the inflow ones $n_\mathrm{int}^\mathrm{I}$ and the outflow contribution $n_\mathrm{int}^\mathrm{O}$. Furthermore, when, for some reason, the flux associated with one of the link related to an internal node is zero, this link has an undetermined orientation. Hence, all the related nodes are also neither inflow or outflow ones. We will call the number of these undetermined nodes n_int^U, so that

$$n_\mathrm{int} = n_\mathrm{int}^\mathrm{I} + n_\mathrm{int}^\mathrm{O} + n_\mathrm{int}^U. \tag{36}$$

Let us also introduce the total number of links n_l associated with the vascular segment between two nodes (or channel between two successive cross-links). These various elements are illustrated in Fig. 2a–c.

In the special case of a network having only bifurcations associated with three links connected to one single internal node, there is a simple relationship between the link and node numbers:

$$2n_{\text{int}}^{\text{I}} + n_{\text{int}}^{\text{O}} + \frac{3}{2} n_{\text{int}}^{U} + n_{\text{i}} = n_l. \tag{37}$$

This relation is easily obtained from spanning along the graph each successive internal node and counting only the outgoing links from each node. A given link is only outgoing for a single node, so that the total number of outgoing links is the total number of links. There are two output links for "inflow" node, I but only one for an "outflow" node O, so that the first two terms on the left-hand side of relation (37) contribute. Furthermore, for two undetermined nodes U, there is a single undetermined link, but there are also two other outgoing links leaving each undetermined node. Hence, for two undetermined nodes U, there are, in fact, three associated links to count among which two are outgoing ones and one is a zero flux undetermined one. Hence, there is a pre-factor $3/2$ before the third left-hand side of (37). Finally, the input nodes have systematically output links associated with them, so that they contribute to the link number. There is no need to count the output nodes n_{o} since they are not associated with any outgoing link.

Let us now discuss how this relation can be used to show that the previous formulations provide a close number of equations for the problem. The pressure problem associated with relation (14) provides n_{int} relations associated with the internal nodes. Furthermore, the boundary conditions associated with the imposed pressure on input and output nodes give $n_{\text{i}} + n_{\text{o}}$ supplementary relations. From (35), it is clear that the problem is closed for the pressure, so that the number of unknowns is equal to the number of equations. Let us now turn to the hematocrit problem. When using the phase separation models, the daughter hematocrit fraction given by the different models (27), (29) or (31) leads to $2n_{\text{int}}^{\text{I}}$ relations for each inflow internal node I for which they are written. On the other outflow internal node O, one has to write the mass conservation (15) which provides $n_{\text{int}}^{\text{O}}$ supplementary relations. Finally, there is a special treatment to be applied to the undetermined node U, which has generally not been given in the previous literature. Since the link relating two undetermined nodes U has zero flux, it can be ignored, and the mass conservation (15) can be trivially applied to each undetermined node U with only two associated outgoing links. Furthermore, one supplementary condition has to be chosen to set the hematocrit value for the undetermined link. There is an arbitrary choice opting for which has no consequence on the final result, and we chose to fix the hematocrit value of undetermined link to zero in the following. This procedure leads to three relations for each pair of undetermined nodes U, which leads to a total of $3/2\ n_{\text{int}}^{U}$ relations. Finally, the input hematocrit conditions associated with the input links are equal to the input nodes n_{i} so that there is a total of $2n_{\text{int}}^{\text{I}} + n_{\text{int}}^{\text{O}} + 3/2\, n_{\text{int}}^{U} + n_{\text{i}}$ relations which from (37) provides the exact number of relations needed to find the hematocrit at each link of the network.

We shall mention as a final remark that the above formulation has not considered the possibility of having undetermined nodes with three null fluxes (which is, in principle, possible). This very special case can easily be handled from isolating this special kind of undetermined node from the network to which it is, in fact, decoupled.

3.1.2 New Formulation

We now propose a new formulation for the problem to be solved for determining the pressure/hematocrit distribution in a complex network. Our main purpose is to show how the mass conservation (15) can be the only relation to consider for determining the hematocrit distribution.

At first, such proposition seems difficult to realize since it has to be written on the internal nodes so that it only provides n_{int} relations which is not enough for determining the n_l hematocrit values at each link. Our main proposition to circumvent this difficulty is to consider a new quantity that we call the *node hematocrit* H_{N_j} defined at each node j of the network. We then define the relationship between this field and the hematocrit which is

$$\Delta_i H_{\text{N}} = H_i, \tag{38}$$

where index i refers to a given oriented link of the network relating two successive nodes, and the Δ_i symbol is the difference between the upstream to downstream node hematocrit field, as used in relation (14). This new *node hematocrit* field can be viewed as a potential for the hematocrit field. It permits to transpose the hematocrit conservation relation from links to nodes, so that the number of equations which are needed to close the problem will then be available, as for the pressure formulation of the flux conservation. (15) can then be rewritten

$$\sum_{i \in J} \Delta_i H_{\text{N}} \frac{\pi}{128} \frac{D_i^4}{\mu_{\text{a}}(\Delta_i H_{\text{N}}, D_i)} \frac{\Delta_i p}{L_i} = 0. \tag{39}$$

This new formulation for mass conservation provides $n_{\text{int}}^{\text{I}} + n_{\text{int}}^{\text{O}}$ relations to the node hematocrit field at each internal node. It is worth mentioning that even if the i index of (39) refers to links, for dimensional quantities D_i, L_i to be evaluated at each link, all the unknowns of H_{N} and p fields are evaluated at the adjacent nodes of the link i based on the evaluations of their adjacent differences using Δ_i operator.

One now has to find the proper boundary conditions to complement this constitutive mass conservation for the node hematocrit field. The input boundary conditions of fixed hematocrit h_0 on each input link related to input nodes can be translated into the following equality:

$$H_{N_j} - H_{N_{\text{i}}} = h_0, \tag{40}$$

where the index j refers to each internal node which is related to an input node i where the node hematocrit is $H_{N_{\text{i}}}$. There is obviously n_{i} relations (40).

A supplementary condition for the output nodes has then to be found. Let us first consider the special case for which there is only one output node $n_{\text{o}} = 1$, as exemplified in Fig. 2a and b. In this special case, the flux in the output link relating the single output node has a known associated flux Q_{tot} which is the total input flux which is injected in the network:

$$Q_{\text{tot}} = \sum_{j \in L_i} Q_j, \tag{41}$$

where L_i is the set of all the links which are related to the n_{i} input nodes. Since this flux is a priori unknown and because it enters in the boundary condition to be applied to the node hematocrit field, this field thus fulfills a *free boundary problem*. We will discuss in the next section the way it could be computed when needed. We will assume here that this total flux is known from solving the pressure problem. Furthermore, the hematocrit of the single output link is also the input hematocrit h_0 which is injected at the input nodes. Thus, the mass conservation associated with the output node where a node hematocrit field $H_{N_{\text{o}}}$ and a pressure value p_{o} can be written

$$-\sum_{j \in N_{\text{o}}} (H_{N_{\text{o}}} - H_{N_j}) \frac{\pi}{128} \frac{D_i^4}{\mu_{\text{a}}(\Delta_i H_{\text{N}}, D_i)} \frac{p_{\text{o}} - p_j}{L_i} = h_0 Q_{\text{tot}}, \tag{42}$$

where N_{o} is the set of all the nodes connected to the single output node o, and index i is related to the links j between output and internal nodes. This supplementary relation permits

to close the problem when there is a single output node $n_o = 1$ since there is a total of $n_{int}^{I} + n_{int}^{O} + n_i + 1$ relations to produce the total number of unknown n which from relation (35) are just enough.
After having found the potential for the hematocrit field at each node H_N which fulfills mass conservation (39), input condition (40), and output condition (42), it is then a direct procedure to deduce the hematocrit field H from relation (38). The hematocrit field H will then automatically fulfill the input condition $H = h_0$ on input nodes, the mass conservation (15), and the mass conservation constraint associated with output links.

Let us now discuss the more complicated case where $n_o > 1$, as illustrated on the example of Fig. 2c. In this case, there is a difficulty since there is no apparent relation between the output nodes to fix a node hematocrit value. Nevertheless, mass conservation still holds for the hematocrit outflux, so that one can define a virtual single output node to impose this outflux mass conservation as illustrated on Fig. 2d. The real output nodes are thus suppressed from the network and replaced by a virtual single output node. The analysis of the previous paragraph can thus apply and relation (42) will provide the unique necessary supplementary relation to close the problem.

3.2 Numerical Implementation

We now describe the numerical implementation of the two theoretical formulations described in the previous sections. They both have the common feature that pressure and hematocrit/node hematocrit are computed independently with a successive iteration procedure. Nevertheless, the hematocrit computation differ from the node hematocrit computation.

3.2.1 Previous Formulations

A successive iteration procedure first used in Pries et al. (1990) is associated with the pressure/hematocrit fields which, at each time step k, is denoted (p^k, H^k). The pressure field is defined on the n network nodes and the hematocrit on the n_l links. The initial value for the hematocrit field is chosen to be uniformly distributed among all the links with the entrance value h_0. Then, the pressure problem p^0 is solved by inverting the linear problem (14) while using the known uniform initial hematocrit field and the applied Dirichlet boundary conditions on nodes n_i and n_o.

Then, the first hematocrit field H^0 is found among the output links of the inflow internal nodes n_{int}^{I} from using one phase separation fractional hematocrit relation among (27), (29) or (31) which propagates the entrance hematocrit values h_0 known on the n_i input nodes using the initial flux Q^0. Furthermore, after exploring all the inflow internal nodes, one then applies to each outflow internal node the mass conservation relation (15). Finally, the n_i input links conditions associated with the input hematocrit h_0 provide the necessary information to find the n_l hematocrit values on the network links.

This procedure is applied iteratively at each order $k > 0$, by replacing the initial uniform hematocrit field by the hematocrit field H^{k-1} obtained in the previous step. The convergence is generally obtained, but it is possible to find some networks for which the convergence does not occur as illustrated in the next section.

3.2.2 New Formulation

We equally proceed with an iterative procedure for (p^k, H_N^k). The difference with the iterative scheme described in the previous section (last paragraph) concerns the second step of

the procedure. Instead of solving the hematocrit problem, we now wish to solve the node hematocrit problem defined in H_{N}^{k}.

For the first step $k = 0$, this node hematocrit is found by inverting the linear system (39) defined on the internal nodes of the network with the pressure field p^0 associated with the first step. This inversion necessitates boundary conditions (40) associated with the input nodes and (42) associated with the output node. The free boundary condition (42) can be found from the knowledge of Q_{tot}^{0} computed at the first step from the known pressure field p^0 and apparent viscosity relations (16) or (20) applied with the initial uniform hematocrit field. It is worth mentioning that the linear system defined by relation (39) and its associated boundary conditions has a non-empty kernel. It is shown in the Appendix that this kernel is indeed associated with the trivial uniform hematocrit solution. The interesting solution associated with a non-uniform hematocrit, complementary to the kernel space, is the one we are interested in. Depending on the method used for the inversion of the linear system (direct or iterative procedure), one should take into account the existence of a trivial kernel (*e.g.* making use of a singular value decomposition method for direct inversion) in the inversion procedure. Finally, the inversion of the linear system for the node hematocrit field H_{N}^{0}, provides the hematocrit field H^0 from relation (38). Each subsequent iterative step can then be performed solving the new pressure problem with the previous hematocrit solution until convergence.

4 Comparison of Phase Separation Models

4.1 Elementary Networks

In this section, we wish to illustrate some interesting specificities of our new formulation as well as pointing out some limitations of the previous models on the most simple possible networks proposed by Carr and Lacoin (2000). For this purpose, we examine two basic configurations which are sketched on the various Figs. 4, 5, 6, 7 and 8. We analyze the most

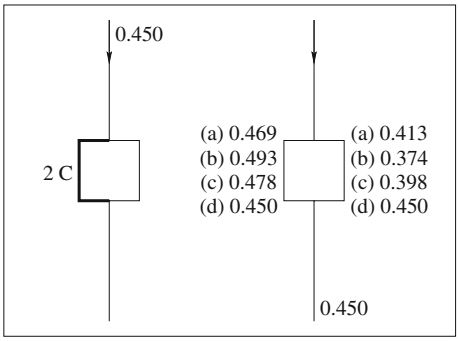

Fig. 4 Plasma skimming results for a simple loop network using the apparent viscosity law of Pries et al. (20) and different models (**a**) Dellimore et al. (27), **b** Fenton et al. (29), **c** Pries et al. (31) and **d** our new approach. The *left figure* indicates the branch where a conductance, which is twice the other one, is chosen. The conductance C is computed using the apparent viscosity model and a uniform hematocrit distribution, so that it is associated with diameter or length differences associated with the branches. The hematocrit values obtained for the different models are indicated on each branch on the *right figure*. The *top* and *bottom values* indicates the hematocrit $H = 0.45$ in the input and output branches

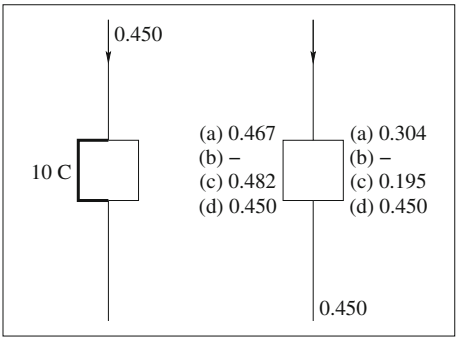

Fig. 5 Same convention as Fig. 4 but using conductance in the *left branch* which is 10 times the value of *right branch*

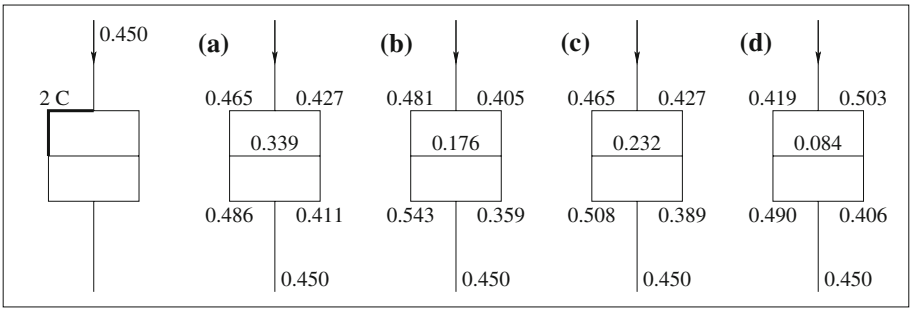

Fig. 6 Same convention as Fig. 4 but with a supplementary inner loop inside the previous one. Each hematocrit values are indicated along each branches. The input hematocrit is still $h_0 = 0.45$

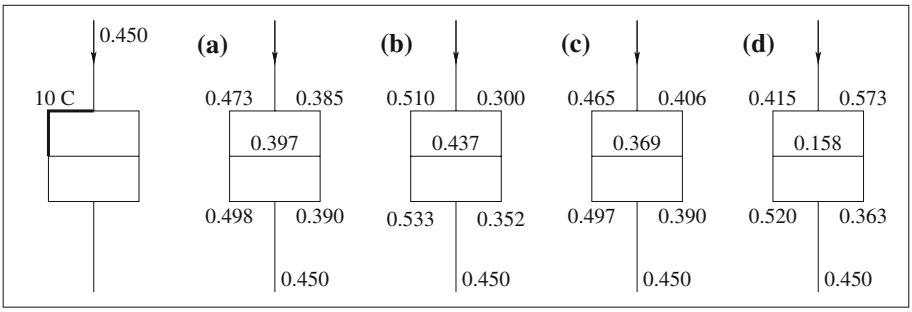

Fig. 7 Same convention as Fig. 6 with a conductance in the left branch which is ten times the value of right branch

simple possible networks which are either a single loop also studied in Pop et al. (2007), or two adjacent ones (similar to a Wheatstone bridge).

Our motivation is to illustrate some non-trivial features of the phase separation models which are more easy to point out on simple networks. Each elementary segment has a $L = 100\,\mu\text{m}$ length, and a $D = 10\,\mu\text{m}$ diameter. We also define the initial conductance C using the above values for D, L and the inlet hematocrit $h_0 = 0.45$. Then, we change tube diameter to break the network symmetry in Figs. 4, 5, 6, 7, 8 and 9 using C, $2\,C$ and $10\,C$. The impact of the different viscosity laws is very weak for these simple networks. Hence, the results of Figs. 4, 5, 6, 7, and 8 are merely identical for the two viscosity laws previously mentioned. We first analyze a non-symmetrical loop on Fig. 4 for which phase separation

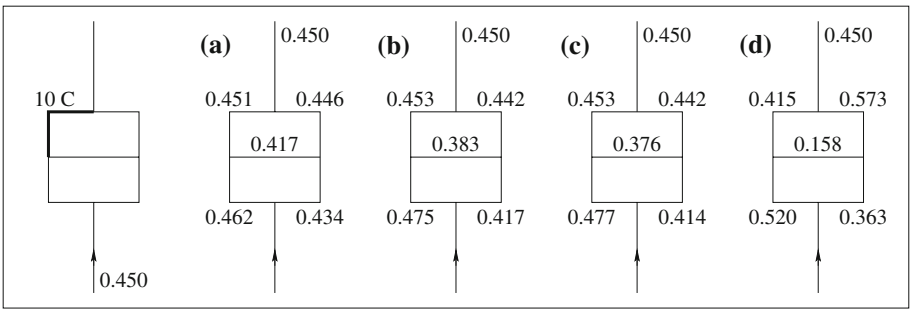

Fig. 8 Same convention as Fig. 7 but with inversion of the flow direction

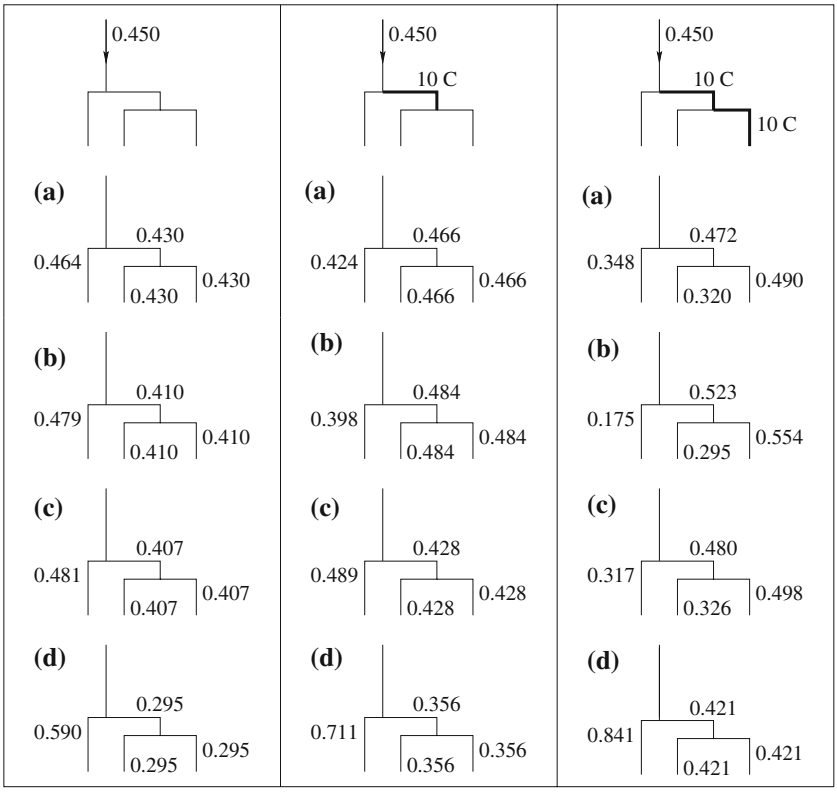

Fig. 9 Plasma skimming in a simple tree-like network. Same conventions as in Fig. 4

models provide a non-symmetrical distribution of the left and right hematocrits. This behavior slightly differs from one model to another, but the observed trend of an increased left-hematocrit and decreased right-hematocrit is similar. On the contrary, our formulation preserves the hematocrit symmetry when considering this very simple network.

When increasing the asymmetry of the network in Fig. 5 by increasing the conductance ratio between the left and right side, the qualitative behavior of the phase separation models is still the same albeit they differ more markedly especially for the value of the right-hand side branch low hematocrit. It turns out that not all phase separation models provide a solution.

Fenton et al.'s model cannot accept this contrasted configuration and does not provide any converged value for the hematocrit field. Again, our formulation does not produce any spatial variation for the hematocrit field. Hence, even for non-symmetrical single loops, the mass conservation prescribed on the output node does not give enough degree of freedom for the hematocrit to change on the right or left branch of a single loop. This homogeneous field result is found even if the fluxes at each internal node bifurcation are non symmetrical. This illustrates the fact that our formulation does not provide a plasma skimming effect from a local balance principle which governs each node. It will rather appear from a more subtle *non local* effect that we now consider.

In the case of the Wheatstone bridge configuration sketched on Fig. 2a, the internal link will experience a zero flux, and thus a zero hematocrit when the bridge is equilibrating, i.e., when the network is symmetrical. Breaking the symmetry of the network will result in a non-zero central flux which brings a non-zero hematocrit. Two symmetry-broken configurations are displayed in Figs. 6, 7, and 8. The first configuration displayed in Fig. 6 is associated with a given link having twice the conductance of the other one as for the single loop configuration illustrated in Fig. 4. The results of the phase separation models exposed in Sect. 2.2.2 are given in Figs. 6a–c. They display the same qualitative trend albeit the results differ quantitatively by a mere factor two for the center's hematocrit value which is found between 0.17 and 0.34. In this case, our model also predicts a non-zero value for the hematocrit which also follows the same trend with nevertheless a much lower amplitude. Increasing the conductance contrast to a factor of 10 does not change much the results obtained with the Dellimore et al.'s model as illustrated in Fig. 7a. It is not the case for the two other phase separation models displayed in Fig. 7b and c for which there is an important increase of the center hematocrit as compared to the one of Fig. 6b and c. A similar increase is also observed with our new formulation in Fig. 7d albeit the hematocrit values differ by a significant amount. Hence, this configuration could be an interesting benchmark for testing the experimental relevance of plasma skimming models, since the value obtained at the center significantly differs from one model to another.

Another interesting comparison between our new formulation and the previous ones is the response to a change in the flow direction. Since our model does not make any difference between inflow and outflow internal nodes, this flow direction should not affect the results given by our model. A more physical interpretation of this property relies on the fact that neither the mass conservation nor the incompressibility are changed by inverting the flow direction. This is not the case for the other models which are highly sensitive to changes in the flow orientation since the inflow internal nodes are changed into outflow nodes and *vice versa*. Such phenomena can be observed in Fig. 8, which is the same configuration as Fig. 7 except for the flow which is directed in the opposite direction. One can observe in those figures that none of the hematocrit computed by our model changes as opposed to all the other models. This is again an interesting property to look at for testing the experimental validity of the proposed model.

4.2 Simple Tree-Like Networks

We now turn to tree-like networks which are interesting structures to consider from different perspectives. They are first more clearly related to physiological networks, albeit very idealized ones. Furthermore, they are also interesting in the context of artificial micro-fluidic networks for which there is generally one single input and output.

Similar to the previous section, we analyze the behavior of the different models when breaking the symmetry of the successive bifurcations of the tree. The left column of Fig. 9

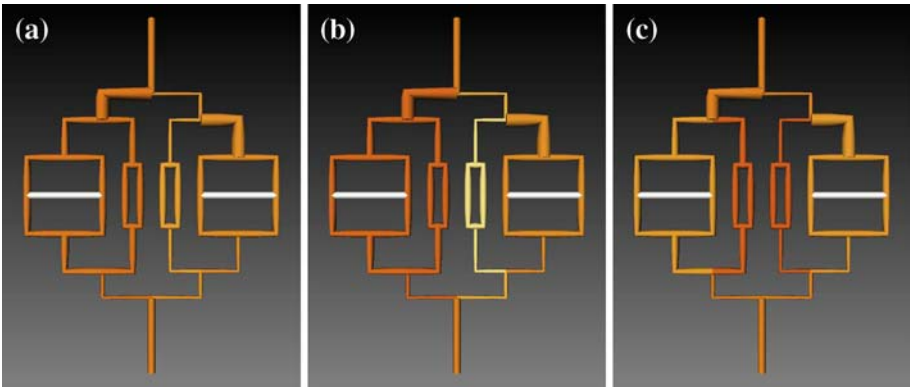

Fig. 10 Plasma skimming in a small network using **a** Dellimore et al. and **b** Fenton et al. phase separation laws. For the same network the fields obtained using our approach is reported in (**c**). Here, Pries et al. viscosity law is used and $h_0 = 0.45$. *Line thickness* symbolizes the vessel diameter. Decreasing colourisation in each branch represents the corresponding hematocrit field from *dark* to *light*

shows the distinct behaviors of the models in a uniform tree having identical conductances in each of its branches. The qualitative trend is that the left branches of this non-symmetrical tree is the same for all models leading to an increase of the hematocrit as compared to the injected value $h_0 = 0.45$. Furthermore, similar behaviors are observed for the different models on the right branches.

When stressing this asymmetry from increasing the conductance of the right side of the tree as done in the second column of Fig. 9, distinct behaviors of the phase separation models occur, some of which decrease the left hematocrit, whilst on the contrary, some others increase it from the initial input value. However, the second branch of the right-hand side of the tree keeps symmetrical values for the hematocrit for all models since it is symmetrical. The third column of Fig. 9 shows that when the asymmetry reaches some extreme value, even the qualitative behavior of our model is distinct from the other ones since the predicted value for the left hematocrit is increased, whereas it is always decreased for all the other models. Furthermore, in our formulation, the right side of the tree keeps a symmetrical response of the hematocrit whereas all the other models display non-symmetrical behavior of their right branches. The behavior of our model (d) in the last third right branch of Fig. 9 is consistent with the result obtained in Fig. 4 where it is found that a simple loop does not provide any hematocrit asymmetry. Since the boundary condition applied at the output nodes illustrated in Fig. 2d leads to a simple loop for the two uppermost right output nodes, it is consistent to find the same value 0.421 for the hematocrit as in the mother branch. This illustrates the influence of the chosen output boundary condition associated with mass conservation at the output nodes.

The variety of different behaviors is finally illustrated in a very idealized convergent–divergent tree similar to that of a "vascular bed," where the changes in branches' diameters are illustrated in Fig. 10. It is interesting to note that the diameters which have been chosen are physiologically relevant, within the range of 5–20 μm. In such a simple network, the phase separation model proposed by Pries et al. does not provide a convergent result. This lack of convergence results from the output given by the separation model (31) for special configurations for which it leads to non-physical hematocrits larger than the one inducing numerical blow-up. Such effect can also occur in very special configurations for all the other models including ours. Nevertheless, it is possible to cure this numerical difficulty by imposing an upper threshold for the hematocrit solution at each link at each successive step. The other

models display rather different behaviors for the hematocrit field as shown in Fig. 10 in colors. The results obtained with the model of Dellimore et al. (27) illustrated in Fig. 10a provide a relative uniform hematocrit field compared with the two others where the diameter's variations have opposing influence, in particular, on the simple loop in the right part of the network.

5 Conclusion

We propose a new approach to model confined suspension flows in complex network. It is based on the formulation of a network approach and conservation principles which can be derived from lubrication approximation for high aspect ratio channels.

The corresponding problem for the pressure/hematocrit is translated into a *non linear free boundary problem* for a new node hematocrit field. This field is defined at each node, and its difference at both end of a given link is the hematocrit. Solution of this new formulation on simple but non-trivial networks have permitted to exhibit a *non-local* origin of phase segregation. More precisely, we have shown that both uniform trivial solution and another non-uniform non-trivial hematocrit field solution fulfil the stationary flux and mass conservation equations when applying uniform input hematocrit boundary conditions. The non-uniform solution is the more interesting one since it is robust to small variations around uniform input concentrations, and since experiments never provide strictly uniform inputs. On the contrary, the trivial solution can only occur for exactly uniform inputs.

The salient properties of our model such as the invariance over directional changes of the flow, sensitivity to broken symmetry, and boundary conditions have been illustrated. We also compare our formulation with previously proposed phenomenological local models for phase separation, and we suggest benchmark configurations for future comparisons with experimental observations.

It is interesting to note that our approach provides a consistent treatment of both the pressure and hematocrit field resolutions. In both cases, local hydrodynamical effects arising in the vicinity of each bifurcation are consistently neglected, since their contribution is small in high aspect ratio channels. This is not the case with previous formulations where the first pressure step neglects local effects whilst the second separation model considers that local effects are an essential explanation for the hematocrit local separation at a bifurcation.

This new approach could be applied to model confined particles suspensions or blood flow distribution in natural or artificial networks, and it might help the design of interesting micro-fluidic networks.

Acknowledgements This study has been supported by GDR No. 2760 "Biomécanique des fluides et des transferts—Interaction fluide/structure biologique," the ASUPS A05 of Paul Sabatier University of Toulouse, France, and the ANR project ANR-06-BLAN-0238-01. FP acknowledges Pr. V. M. Entov for his very nice discussions in DAMTP (Cambridge) on Non-newtonian fluids and Russian scientists.

Appendix

In this appendix, we give an explicit form for the discrete numerical implementation of our new formulation. We then show that the kernel associated with the linear operator is related to the trivial homogeneous hematocrit solution.

Let us consider the node hematocrit field $\mathbf{H_N}$ as a vector which is structured from first considering the input nodes components $\mathbf{H_N^I}$, and then the internal nodes components $\mathbf{H_N^{int}}$ ordered so that those adjacent to an input node are listed first, and then (possibly virtual) single output node H_N^O. Then $\mathbf{H_N}$ reads

$$\mathbf{H_N} = \left(\frac{\mathbf{H_N^I}}{\frac{\mathbf{H_N^{int}}}{H_N^O}} \right). \tag{43}$$

The linear system applied to this hematocrit field associated with relation (39), input condition (40), and output condition (42) can be implemented in the following way:

$$\mathbf{A} \cdot \mathbf{H_N} = \mathbf{b}, \tag{44}$$

with,

$$A = \left(\frac{\mathbf{I} \mid -\mathbf{I} \mid 0}{\mathbf{Q}} \right). \tag{45}$$

where $\mathbf{I}$ designs the identity matrix, and $\mathbf{Q}$ the flux matrix. $\mathbf{Q}$ is a rectangular matrix associating the flux at each link with their adjacent nodes. It is known at each step of the iterative procedure described in the second paragraph of Sect. 3.2. Q_{ij} is thus the assigned flux arising between node i and node j regardless of whether these nodes are inputs, internal or outputs. By construction $Q_{ij} = -Q_{ji}$. The second member vector $\mathbf{b}$ is

$$\mathbf{b} = h_0 \left(\frac{\mathbf{1}}{\frac{\mathbf{0}}{-Q_{\text{tot}}}} \right). \tag{46}$$

where $\mathbf{1}$ and $\mathbf{0}$ are the vectors whose components are all equal to 1 and 0 and associated with input and internal nodes, respectively.

Let us now show that the kernel of the linear system (44) is associated with the trivial solution $H_i = h_0$.

For this, let us consider an auxiliary hematocrit field which is just a translation of the original one $H_i' = H_i - h_0$. Similarly, one can define the auxiliary node hematocrit $\mathbf{H_N'}$ associated with this auxiliary field $\mathbf{H'}$. Since the translation does not affect the node difference, $\mathbf{H_N'} = \mathbf{H_N}$. Hence, the constitutive relations associated with $\mathbf{H_N'}$ are the same as those for $\mathbf{H_N}$, i.e., (39). However, the input condition (40) and output condition (42) for $\mathbf{H_N'}$ should be considered with $h_0 = 0$. Hence, for the linear system (44) associated to the auxiliary field $\mathbf{H_N'}$, $\mathbf{b} = \mathbf{0}$ since h_0 factorizes the right-hand side of relation (46). The kernel of matrix $\mathbf{A}$ associated with the mass conservation relation (14) provides a node hematocrit field $\mathbf{H_N'}$ which equals a constant everywhere. This single degree of freedom kernel is one-dimensional and leads to $\mathbf{H'} = \mathbf{0}$, or $H_i = h_0$, i.e., the trivial uniform solution.

References

Barenblatt, G.I., Entov, V.M., Ryzhik, V.M.: Theory of Fluid Flows Through Natural Rocks. Kluwer, Dordrecht (1990)

Carr, R.T., Lacoin, M.: Nonlinear dynamics of microvascular blood flow. Ann. Biomed. Eng. **28**, 641–652 (2000)

Carr, R.T., Geddes, J.B., Wu, F.: Oscillations in a simple microvascular network. Ann. Biomed. Eng. **33**(6), 764–771 (2005)

Chien, S., Tvetenctrand, C.D., Farrel Epstein, M.A., Schmid-Schönbein, G.W.: Model studies on distributions of blood cells at microvascular bifurcations. Am. J. Physiol. Heart Circ. Physiol. **248**, 568–576 (1985)

Cokelet, G.R.: Viscometric, in vitro and in vivo blood viscosity relationships: how are they related?. Biorheology **36**, 343–358 (1999)

Damiano, E.R., Duling, B.R., Ley, K., Skalak, T.C.: Axisymmetric pressure-driven flow of rigid pellets through a cylindrical tube lined with a deformable porous wall layer. J. Fluid Mech. **314**, 163–189 (1996)

Dellimore, J.W., Dunlop, M.J., Canham, P.B.: Ratio of cells and plasma in blood flowing past branches in small plastic channels. Am. J. Physiol. Heart Circ. Physiol. **244**, 635–643 (1983)
Devor, A., Hillman, E.M.C., Tian, P., Waeber, C., Teng, I.C., Ruvinskaya, L., Shalinsky, M.H., Zhu, H., Haslinger, R.H., Narayanan, S.N., Ulbert, I., Dunn, A.K., Lo, E.H., Rosen, B.R., Dale, A.M., Kleinfeld, D., Boas, D.A.: Stimulus-induced changes in blood flow and 2-deoxyglucose uptake dissociate in ipsilateral somatosensory cortex. J. Neurosci. **28**(53), 14347–14357 (2008)
El-Kareh, A.W., Secomb, T.W.: A model for red blood cell motion in bifurcating microvessels. Int. J. Multiph. Flow **26**, 1545–1564 (2000)
Enden, G., Popel, A.S.: A numerical study of plasma skimming in small vascular bifurcations. J. Biomech. Eng. **116**, 79–88 (1994)
Entov, V.M., Rozhkov, A. N.: Elastic effects in the flow of polymer solutions in channels of variable cross section and a porous medium. J. Eng. Phys. Thermophys. **49**(3), 1032–1038 (1985)
Fåhræus, R., Lindquist, T.: The viscosity of blood in narrow capillary tubes. Am. J. Physiol. **96**, 562–568 (1931)
Faivre, M., Abkarian, M., Bickra, K., Stone, H.A.: Geometrical focusing of cells in a microfluidic device: an approach to separate blood plasma. Biorheology **43**(2), 147–155 (2006)
Feng, J., Weinbaum, S.: Lubrication theory in highly compressible porous media: the mechanics of skiing, from red cells to humans. J. Fluid Mech. **422**, 281–317 (2000)
Fenton, B.M., Carr, R.T., Cokelet, G.R.: Nonuniform red cell distribution in 20 to 100 μm bifurcations. Microvasc. Res. **29**, 103–126 (1985a)
Fenton, B.M., Wilson, D.W., Cokelet, G.R.: Analysis of the effects of mearsured white blood cell entrance times on hemodynamics in a computer model of microvascular bed. Pflüg. Arch. Eur. J. Physiol **403**, 396–401 (1985b)
Fung, Y-.C.: Stochastic flow in capillary blood vessels. Microvasc. Res. **5**, 34–48 (1973)
Kiani, M.F., Hudetz, A.G.: A semi-empirical model of apparent blood viscosity as a function of vessel diameter and discharge hematocrit. Biorheology **28**, 65–73 (1991)
Kiani, M.F., Pries, A.R., Hsu, L.L., Sarelius, I.H., Cokelet, G.R.: Fluctuations in microvascular blood flow parameters caused by hemodynamic mechanisms. Am. J. Physiol. Heart Circ. Physiol. **266**, 1822–1828 (1994)
Kleinfeld, D., Mitra, P.P., Helmchen, F., Denk, W.: Fluctuations and stimulus-induced changes in blood flow observed in individual capillaries in layers 2 through 4 of rat neocortex. Proc. Natl Acad. Sci. USA **95**, 15741–15746 (1998)
Leal, L.G.: Laminar flow and convective transport processes. Butterworth-Heinemann Ltd, Boston (1992)
Lee, J., Smith, N.P.: Theoretical modeling in hemodynamics of microcirculation. Microcirculation **15**, 699–714 (2008)
Lighthill, M.J.: Pressure-forcing of tightly fitting pellets along fluid-filled elestic tubes. J. Fluid Mech. **34**(1), 113–143 (1968)
McWhirter, J.L., Noguchia, H., Gomppera, G.: Flow-induced clustering and alignment of vesicles and red blood cells in microcapillaries. Proc. Natl Acad. Sci. **106**(15), 6039–6043 (2009).
Plouraboué, F., Flukiger, F., Prat, M., Crispel, P.: Geodesic network method for flows between two rough surfaces in contact. Phys. Rev. E **73**, 036305 (2006)
Pop, S.R., Richardson, G., Waters, S.L., Jensen, O.E.: Shock formation and non-linear dispersion in a microvascular capillary network. Math. Med. Biol. **24**, 379–400 (2007)
Popel, A.S., Johnson, P.C.: Microcirculation and hemorheology. Annu. Rev. Fluid Mech. **37**, 43–69 (2005)
Popel, A.S., Liu, A., Dawant, B., Koller, A., Johnson, P.C.: Distribution of vascular resistance in terminal arteriolar networks of cat sartorius muscle. Am. J. Physiol. Heart Circ. Physiol. **254**, 1149–1156 (1988)
Pries, A.R., Ley, K., Gaehtgens, P.: Generalization of the Fåhræus principle for microvessel networks. Am. J. Physiol. Heart Circ. Physiol. **251**, 1324–1332 (1986)
Pries, A.R., Ley, K., Claassen, M., Gaehtgens, P.: Red cell distribution at microvascular bifurcations. Microvasc. Res. **38**(1), 81–101 (1989)
Pries, A.R., Secomb, T.W., Gaehtgens, P., Gross, J.F.: Blood flow in microvascular networks—experiments and simulation. Circ. Res. **67**, 826–834 (1990)
Pries, A. R., Neuhaus, D., Gaehtgens, P.: Blood viscosity in tube flow: dependence on diameter and hematocrit. Am. J. Physiol. Heart Circ. Physiol. **263**, 1770–1778 (1992)
Pries, A.R., Secomb, T.W., Gaehtgens, P.: Biophysical aspects of blood flow in the microvasculature. Cardiovasc. Res. **32**, 654–667 (1996)
Quéguiner, C., Barthès-Biesel, D.: Axisymmetric motion of capsules through cylindrical channels. J. Fluid Mech. **348**, 349–376 (1997)
Risser, L., Plouraboué, F., Cloetens, P., Fonta, C.: A 3D investigation shows that angiogenesis in primate cerebral cortex mainly occurs at capillary level. Int. J. Dev. Neurosci. **27**(2), 185–196 (2009)